Matrix Isolation Infrared Spectroscopic and Theoretical Studies on the Reactions of Manganese and Iron Monoxides with Methane

Guanjun Wang, Mohua Chen, and Mingfei Zhou*

Department of Chemistry & Laser Chemistry Institute, Shanghai Key Laboratory of Molecular Catalysts and Innovative Materials, Fudan University, Shanghai 200433, People's Republic of China

Received: August 16, 2004; In Final Form: October 11, 2004

The reactions of manganese and iron monoxides (MnO and FeO) with methane molecules have been investigated using matrix isolation infrared absorption spectroscopy. The metal monoxide molecules were prepared by laser ablation of MnO_2 or Fe_2O_3 targets. The reaction products were identified on the basis of isotopic substitution experiments with $^{13}CH_4$ and CD_4, as well as density functional theoretical calculations. In solid argon, manganese and iron monoxides reacted with methane spontaneously on annealing to form the $OMn(CH_4)$ and $OFe(CH_4)$ complexes, which were predicted to have C_{2v} symmetry with the metal atom coordinated to two hydrogen atoms of the methane molecule. The $OMn(CH_4)$ and $OFe(CH_4)$ complexes underwent photochemical rearrangement to the CH_3MnOH and CH_3FeOH molecules upon ultraviolet irradiation.

Introduction

The catalytic conversion of methane to methanol has gained much attention due to its great economic and scientific importance.[1] The $CH_4 + MO^+ \rightarrow M^+ + CH_3OH$ reaction is of particular interest since this process is viewed as the simplest model for alkane hydroxylation. Previous experimental studies have been focused on the gas phase reactions of various transition metal oxide ions with methane.[2−5] Schröder, Schwarz, and co-workers have systematically investigated the gas phase reactions of the first row transition metal monoxide ions and methane, demonstrating that late transition metal monoxide ions can efficiently convert methane to methanol while the early transition metal monoxide ions cannot.[2] In an $FeO^+ + CH_4$ reaction study, an $HOFe^+CH_3$ species has been suggested as a key intermediate in the reaction process.[3] Metz and co-workers have prepared the $HOFe^+CH_3$ and $CH_2FeOH_2^+$ intermediates in the $FeO^+ + CH_4$ reaction in the jet by ion molecular reactions, and their photodissociation has been examined in the visible and near-UV range using time-of-flight mass spectrometry.[5] Theoretically, Yoshizawa and co-workers have calculated the reaction pathway and energetics for methane-to-methanol conversion by first row transition metal monoxide ions.[6] The $MO^+ + CH_4 \rightarrow M^+ + CH_3OH$ reactions were suggested to proceed via the initial formation of an $OM^+(CH_4)$ complex followed by isomerization to the HOM^+CH_3 and $M^+(CH_3OH)$ intermediates via two transition states. The results showed that the experimentally observed reaction efficiency and methanol-to-methyl branching ratio could be rationalized in terms of the predicted barrier heights at the transition states. The reactivities of different iron−oxo species FeO^{n+} ($n = 0, 1, 2$) toward methane were also computed by Yoshizawa et al., and it was found that the iron(IV)−oxo species are most effective for the cleavage of the C−H bond of methane.[7]

The reaction of neutral transition metal oxides with methane has received much less attention. Broclawik et al. have investigated the interaction of palladium monoxide with methane by means of density functional theory, and found that palladium monoxide can form a weak complex bound by 3.3 kcal/mol. The insertion of PdO into the C−H bond of methane to form CH_3PdOH was predicted to have an energy barrier of 24.5 kcal/mol.[8,9] The reactions of scandium, nickel, and palladium monoxides with methane were also studied by Hwang and Mebel using density functional calculations.[10,11] Similar to the transition metal monoxide ions, neutral NiO and PdO are reactive toward methane and can form molecular complexes with CH_4 bound by 8−9 kcal/mol without a barrier. At elevated temperatures, the dominant reaction channel is direct abstraction of a hydrogen atom by the oxides from CH_4 with a barrier of 16 kcal/mol. The insertion into a C−H bond to produce CH_3-MOH is a minor reaction channel and proceeds via a transition state lying 19−20 kcal/mol above the initial reactants. On the contrary, the results showed that ScO is not reactive with respect to methane at low and ambient temperatures. Goddard and co-workers investigated the methane activation by MO_x (M = Cr, Mo, W; $x = 1, 2, 3$), and found that the trends in reactivity can be rationalized in terms of changes in electrophilicity of MO_x, the strength of the M−O π bonds, and the binding properties of MO_x to methyl or hydrogen.[12] These theoretical studies have provided valuable information concerning the reaction mechanism and energetics.

In this paper, we report a combined matrix isolation infrared absorption spectroscopic and theoretical study of the reactions of neutral MnO and FeO with methane. The reaction intermediates and products were trapped and characterized.

Experimental and Theoretical Methods

The experimental setup for pulsed laser ablation and matrix isolation FTIR spectroscopic investigation has been described in detail previously.[13] Briefly, the 1064 nm Nd:YAG laser fundamental (Spectra Physics, DCR 150, 20 Hz repetition rate and 8 ns pulse width) was focused onto the rotating MnO_2 or Fe_2O_3 targets, which were prepared by sintered metal oxide powders. The ablated species were co-deposited with methane in excess argon onto a 12 K CsI window for 2 h at a rate of

* Corresponding author. E-mail: mfzhou@fudan.edu.cn.

10.1021/jp046324h CCC: $27.50
Published on Web 11/24/2004

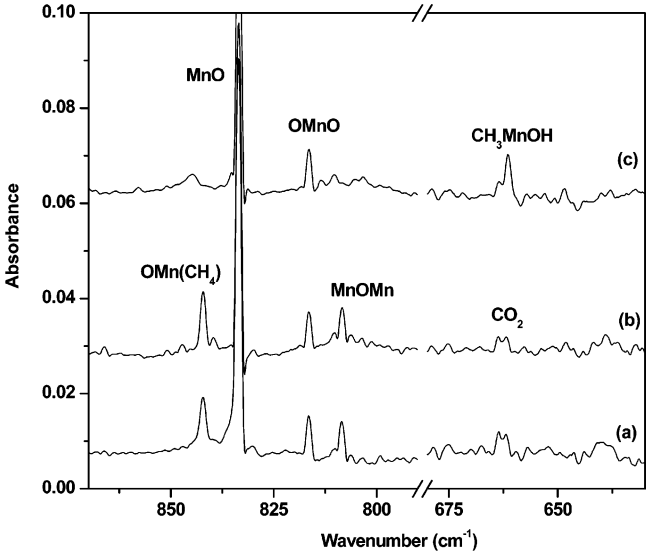

Figure 1. Infrared spectra in 870−790 and 680−630 cm^{-1} regions from co-deposition of laser-ablated MnO_2 target with 0.8% CH_4 in excess argon. (a) 2 h of sample deposition at 12 K, (b) after 30 K annealing, and (c) after 30 min of broad-band irradiation.

approximately 2−4 mmol/h. Isotopically labeled CD_4 (Isotec, 99%), $^{13}CH_4$ (Isotec, 99%), and mixtures were used in different experiments. Infrared spectra were recorded on a Bruker IFS 113 V spectrometer at 0.5 cm^{-1} resolution using a DTGS detector. Matrix samples were annealed at different temperatures, and selected samples were subjected to broad-band irradiation using a 250 W high-pressure mercury arc lamp and glass filters.

Density functional calculations were performed using the Gaussian 98 program.[14] The three-parameter hybrid functional according to Becke with additional correlation corrections due to Lee, Yang, and Parr (B3LYP) was utilized.[15,16] The 6-311++G** basis set was used for H, C, and O atoms, and the all-electron basis set of Wachters−Hay as modified by Gaussian was used for Fe and Mn atoms.[17,18] The geometries were fully optimized and the stability of the electronic wave function was tested; the harmonic vibrational frequencies were calculated with analytic second derivatives and zero point energies (ZPE) were derived. Transition state optimizations were done with the synchronous transit-guided quasi-Newton (STQN) method[19] at the B3LYP/6-311++G** level followed by the vibrational frequency calculations showing the obtained structures to be true saddle points.

Results and Discussion

Infrared Spectra. The MnO and FeO reactants were prepared from laser ablation of MnO_2 and Fe_2O_3 targets. Under controlled ablation laser energy, laser ablation of a MnO_2 target followed by condensation with pure argon formed MnO (833.3 cm^{-1}) as the major product with minor MnO_2 (948.0 and 816.4 cm^{-1}) and MnOMn (808.3 cm^{-1}).[20] Distinct new product absorptions were observed in experiments using CH_4/Ar as reagent gas. Figure 1 shows the representative spectra in selected regions with a CH_4/Ar sample (0.8% molar ratio), and the product absorptions are listed in Table 1. Besides the manganese oxide absorptions, a new band at 842.1 cm^{-1} was observed on sample deposition. This band increased slightly on 30 K annealing and disappeared on subsequent broad-band irradiation, during which a new band at 661.4 cm^{-1} was produced. A weak band at 1616.5 cm^{-1} (not shown in Figure 1), which was previously assigned to the $HMnCH_3$ molecule, was also observed in the experiment

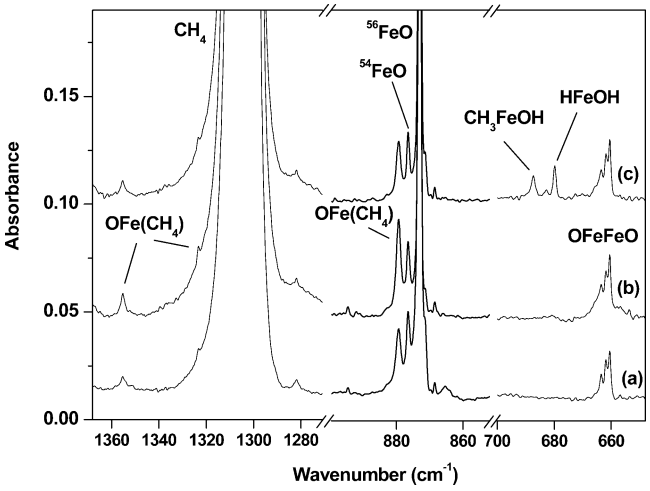

Figure 2. Infrared spectra in 1370−1270, 900−850, and 700−650 cm^{-1} regions from co-deposition of laser−ablated Fe_2O_3 target with 0.8% CH_4 in excess argon. (a) 2 h of sample deposition at 12 K, (b) after 30 K annealing, and (c) after 30 min of broad-band irradiation.

TABLE 1: Infrared Absorptions (cm^{-1}) from MO + CH_4 Reactions in Solid Argon

CH_4	$^{13}CH_4$	CD_4	assignment
842.1	842.1	843.0	$OMn(CH_4)$, ν(Mn−O)
661.4	660.5	643.9	CH_3MnOH, ν(Mn−OH)
1355.2	1348.4	1021.3	$OFe(CH_4)$, $\delta(CH_2)$
1323.3	1315.8	1007.6	$OFe(CH_4)$, $\delta(CH_2)$
879.4	879.4	879.3	$OFe(CH_4)$, ν(Fe−O)
		2759.8	CD_3FeOD, ν(O−D)
687.4	686.8	667.2	CH_3FeOH, ν(Fe−OH)

after broad-band irradiation.[21] In some experiments, the HMnOH molecule (1663.4 and 648.6 cm^{-1}) formed from the reaction of Mn atom with trace H_2O impurity was also observed.[22]

Similar experiments were also performed using the Fe_2O_3 target. Co-deposition of the species from laser ablation of Fe_2O_3 with argon at 12 K produced strong iron monoxide absorption (FeO, 872.8 cm^{-1}) and weak other metal oxide absorptions (FeO_2, 945.8 and 797.0 cm^{-1}; OFeFeO, 661.5, 660.6 cm^{-1}).[23] As shown in Figure 2, new absorptions at 1355.2, 1323.3, and 879.4 cm^{-1} were observed when the species from laser ablation of Fe_2O_3 were co-deposited with CH_4 in excess argon (Figure 2a). These three new absorptions increased on sample annealing to 30 K (Figure 2b), but decreased on subsequent broad-band irradiation (Figure 2c), during which a new band at 687.4 cm^{-1} was produced. Weak bands due to $HFeCH_3$ (1683.6 cm^{-1}) and HFeOH (1731.0 and 679.7 cm^{-1}) formed from the reactions of Fe atoms with methane and H_2O were also observed upon broad-band irradiation.[24,25]

Experiments were repeated with the $^{13}CH_4$, CD_4, and CH_4 + CD_4 samples. The isotopic frequencies are also listed in Table 1. The infrared spectra in selected regions using different isotopic samples are shown in Figures 3, 4, and 5, respectively.

Calculation Results. DFT/B3LYP calculations were performed on the potential reaction products. Three $OMCH_4$ (M = Mn, Fe) isomers, namely, the $OM(CH_4)$ complex, the inserted CH_3MOH molecule, and the $M(CH_3OH)$ complex, were considered. Both quintet and triplet states of the $OFeCH_4$ isomers were optimized. The results showed that the quintet state is more stable than the triplet state for all three isomers. For the OMn + CH_4 system, both sextet and quartet states were optimized, and it was found that the sextet state is the ground state for all three $OMnCH_4$ isomers. The optimized geometric parameters

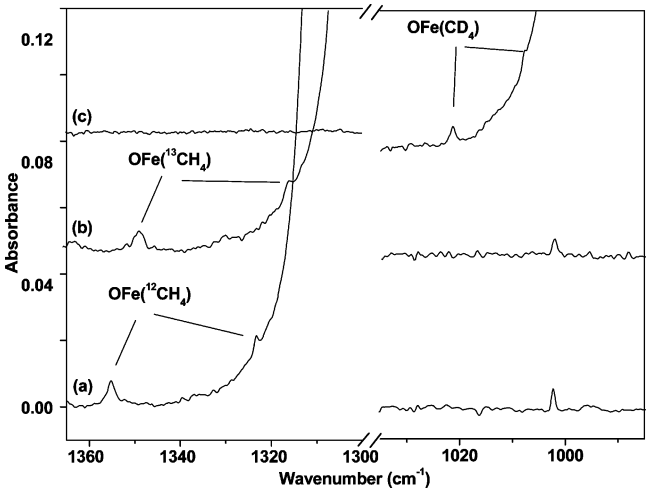

Figure 3. Infrared spectra in 1370−1300 and 1035−985 cm^{-1} regions from co-deposition of laser-ablated Fe_2O_3 target with isotopically substituted CH_4 in excess argon. Spectra were taken after 2 h of sample deposition followed by 30 K annealing. (a) 0.8% CH_4, (b) 0.8% $^{13}CH_4$, and (c) 0.8% CD_4.

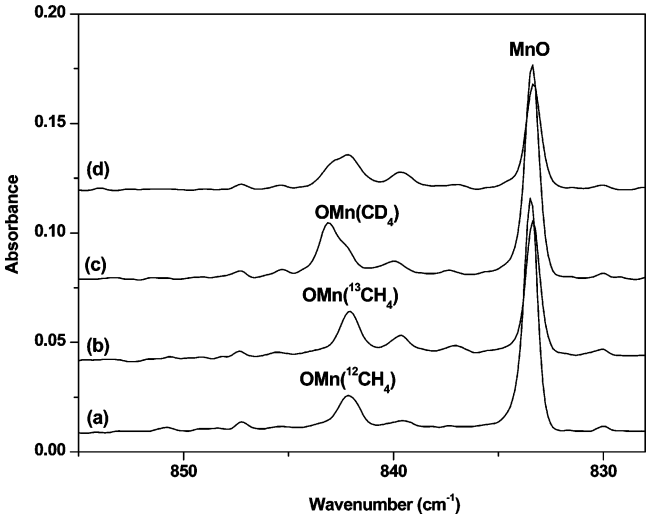

Figure 4. Infrared spectra in 855−828 cm^{-1} region from co-deposition of laser-ablated MnO_2 target with isotopically substituted CH_4 in excess argon. Spectra were taken after 2 h of sample deposition followed by 30 K annealing. (a) 0.8% CH_4, (b) 0.8% $^{13}CH_4$, (c) 0.8% CD_4, and (d) 0.4% CH_4 + 0.4% CD_4.

for the ground state $OMCH_4$ isomers are shown in Figure 6, and the vibrational frequencies and intensities are listed in Table 2.

$OM(CH_4)$. The 1355.2, 1323.3, and 879.4 cm^{-1} bands in the Fe_2O_3 + CH_4 experiments exhibited the same relative intensities in experiments with different laser energy and CH_4 concentrations, suggesting that these three bands are due to different vibrational modes of the same molecule. The 1355.2 and 1323.3 cm^{-1} bands shifted to 1348.4 and 1315.8 cm^{-1} with $^{13}CH_4$ and to 1021.3 and 1007.6 cm^{-1} with CD_4; they gave isotopic frequency ratios of 1.0050 and 1.0057 for $^{12}C/^{13}C$ and 1.3269 and 1.3133 for H/D, respectively. These ratios are very close to those of the CH_2 deformation mode of methane (observed at 1305.4 cm^{-1}) and the $OSc(CH_4)$ complex.[26] The band positions and isotopic frequency ratios suggest the assignment of these two bands to the CH_2 deformation modes of a CH_4 complex. In the mixed CH_4 + CD_4 experiment, no intermediate absorption was observed, indicating that only one CH_4 subunit is involved. The 879.4 cm^{-1} band is only 6.6 cm^{-1} higher than the Fe−O stretching frequency of FeO in solid argon; it exhibited no shift with $^{13}CH_4$ and a very small shift (0.1 cm^{-1}) with CD_4, which suggests that this band is most likely due to the terminal Fe−O stretching vibration of an FeO complex. Accordingly, we assign the 1355.2, 1323.3, and 879.4 cm^{-1} bands to the CH_2 deformation and Fe−O stretching vibrations of the $OFe(CH_4)$ complex.

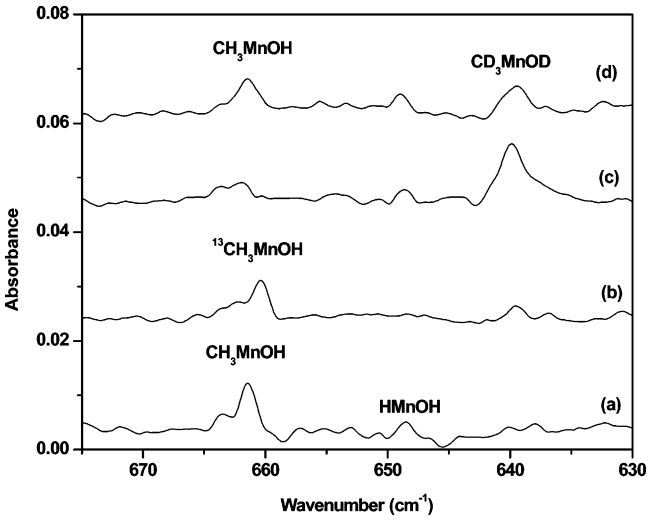

Figure 5. Infrared spectra in 675−630 cm^{-1} region from co-deposition of laser-ablated MnO_2 target with isotopically substituted CH_4 in excess argon. Spectra were taken after 2 h of sample deposition followed by 30 K annealing and 30 min of broad-band irradiation. (a) 0.8% CH_4, (b) 0.8% $^{13}CH_4$, (c) 0.8% CD_4, and (d) 0.4% CH_4 + 0.4% CD_4.

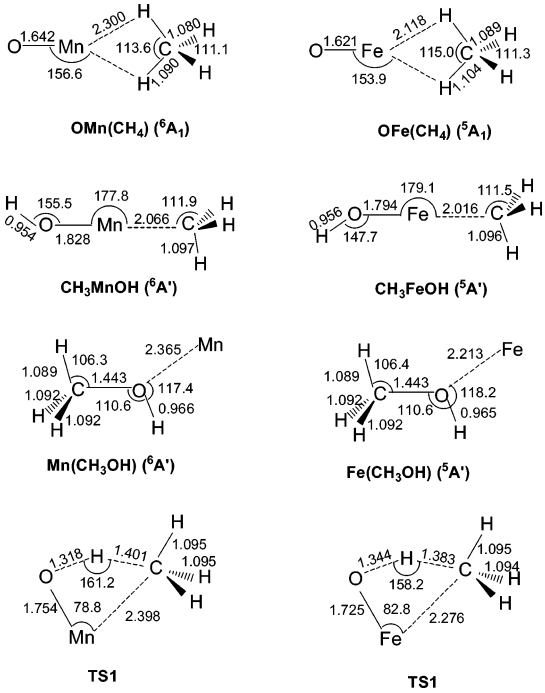

Figure 6. Optimized structures (bond lengths in Å, bond angles in deg) of ground state $OMnCH_4$ and $OFeCH_4$ isomers, and transition states (TS1).

The assignment was supported by density functional calculations. As shown in Figure 6, the $OFe(CH_4)$ complex was predicted to have a $^5A_1$ ground state with C_{2v} symmetry. The iron atom of FeO is coordinated to the two hydrogen atoms of CH_4 (i.e., η^2-CH_4 bonding). Upon complex formation, the structure of the methane unit is deformed from the T_d-type geometry of free methane into the C_{2v} structure. The binding

TABLE 2: Calculated Vibrational Frequencies (cm^{-1}) and Intensities (km/mol) of Experimentally Observed $OM(CH_4)$ and CH_3MOH (M = Mn and Fe) Molecules at the B3LYP/6-311++G Level**

molecule	frequency (intensity)
$OFe(CH_4)$ ($^5A_1$)	3166.1 (0), 3107.8 (7), 2982.9 (3), 2898.6 (19), 1582.7 (9), 1532.7 (0), 1390.3 (48), 1361.8 (17), 1253.8 (11), 914.7 (205), 359.5 (0), 189.1 (2), 151.2 (2), 103.2 (15), 67.8 (15)
CH_3FeOH (^5A)	3957.9 (126), 3061.9 (17), 3061.2 (17), 2994.9 (11), 1445.2 (1), 1443.0 (1), 1202.2 (9), 701.3 (198), 590.4 (42), 588.3 (42), 509.0 (14), 271.6 (153), 111.1 (59), 97.3 (8), 67.3 (83)
$OMn(CH_4)$ ($^6A_1$)	3158.9 (1), 3106.6 (21), 3030.0 (3), 2950.4 (42), 1564.7 (6), 1536.7 (0), 1374.7 (42), 1346.3 (17), 1269.7 (6), 888.1 (259), 229.0 (1), 126.7 (8), 125.3 (7), 83.6 (16), 53.8 (10)
CH_3MnOH (^6A)	3975.3 (109), 3057.9 (18), 3056.7 (18), 2992.6 (17), 1449.2(0), 1448.7 (1), 1197.3 (6), 679.3 (199), 586.4 (42), 585.3 (45), 490.7 (8), 206.6 (148), 97.6 (0), 92.0 (12), 42.3 (147)

energy of $OFe(CH_4)$ with respect to $FeO + CH_4$ was predicted to be 4.8 kcal/mol at the B3LYP/6-311++G** level after zero point energy corrections. The CH_2 deformation and Fe−O stretching frequencies were predicted at 1390.3, 1361.8, and 914.7 cm^{-1}, which are in good agreement with the experimental values. These three modes were predicted to have 48, 17, and 205 km/mol IR intensities. All of the other vibrational modes have lower IR intensities (Table 2), and were not observed in the experiments. The calculated isotopic frequency ratios for the CH_2 deformation mode ($^{12}C/^{13}C$, 1.0053 and 1.0060; H/D, 1.3358 and 1.3252) fit the experimental values very well.

The 842.1 cm^{-1} band in the $MnO_2 + CH_4$ experiments is assigned to the Mn−O stretching mode of the $OMn(CH_4)$ complex following the example of $OFe(CH_4)$. This band had no carbon-13 isotopic shift with $^{13}CH_4$, but blue-shifted to 843.0 cm^{-1} in the CD_4 experiment. The band position is 8.8 cm^{-1} higher than that of diatomic MnO in solid argon. The CH_2 deformation mode of the $OMn(CH_4)$ complex was not observed. Similar to the $OFe(CH_4)$ complex, the $OMn(CH_4)$ complex was predicted to have a $^6A_1$ ground state with C_{2v} symmetry. It was predicted to be bound by 1.9 kcal/mol with respect to the ground state $MnO + CH_4$. This binding energy is lower than that of the $OFe(CH_4)$ complex, suggesting that the interaction between MnO and CH_4 is weaker than the interaction between FeO and CH_4. As listed in Table 2, the Mn−O stretching mode was calculated at 888.1 cm^{-1}, blue-shifted 20.3 cm^{-1} from that of MnO (867.8 cm^{-1}) calculated at the same level. The CH_2 deformation mode was predicted at 1374.7 cm^{-1} with an intensity about 16% of the Mn−O stretching mode. This mode may either be overestimated or overlapped by the strong CH_4 absorption.

CH_3MOH. In the $Fe_2O_3 + CH_4$ experiment, the band at 687.4 cm^{-1} was produced after broad-band irradiation, during which the $OFe(CH_4)$ absorptions decreased. This band shifted to 686.8 cm^{-1} with $^{13}CH_4$ and to 667.2 cm^{-1} with CD_4. The band position and H/D isotopic frequency ratio (1.0303) imply that this band is due to an Fe−OH stretching vibration. This band is assigned to the Fe−OH stretching mode of CH_3FeOH according to the isotopic experiments and a previous report.[27] The CH_3FeOH molecule has been produced and characterized in the reaction of $Fe + CH_3OH$. Two bands at 3744.8 and 687.5 cm^{-1} have been assigned to the O−H and Fe−OH stretching modes of the CH_3FeOH molecule in solid argon.[27] The O−H stretching mode of CH_3FeOH could not be observed in our experiment due to weakness, but this mode of the CD_3OD isotopomer was clearly observed at 2759.8 cm^{-1}. As shown in Figure 6, the CH_3FeOH molecule was predicted to have a $^5A'$ ground state with C_s symmetry. The O−H and Fe−OH stretching vibrational frequencies of CH_3FeOH were predicted at 3957.3 and 701.3 cm^{-1}. The calculated isotopic frequency ratios for the Fe−OH stretching mode ($^{12}C/^{13}C$, 1.0007; and H/D, 1.0278) also match the observed values ($^{12}C/^{13}C$, 1.0009; and H/D, 1.0303).

Similarly, a band at 661.4 cm^{-1} in the $MnO_2 + CH_4$ experiments appeared only upon broad-band irradiation and is assigned to the Mn−OH stretching mode of the CH_3MnOH molecule. This band shifted to 643.9 cm^{-1} in the CD_4 experiment and gave a H/D ratio of 1.0336. The band position and isotopic H/D ratio are close to those of the Mn−OH stretching mode of HMnOH (648.6 cm^{-1} with a H/D ratio of 1.0317).[22] The 661.4 cm^{-1} band exhibited 0.9 cm^{-1} isotopic shift when the $^{13}CH_4$ reactant was used, indicating that this vibration mode was weakly perturbed by the CH_3 subunit. The CH_3MnOH molecule was found to have a $^6A'$ ground state with a strong Mn−OH stretching vibration at 679.3 cm^{-1}. The $^{13}CH_3MnOH$ and CD_3MnOD isotopomers were predicted to absorb at 678.9 and 661.2 cm^{-1}, respectively.

Reaction Mechanism. Laser ablation of the MnO_2 and Fe_2O_3 targets produces metal monoxides (MnO and FeO) as the major products. The $OMn(CH_4)$ and $OFe(CH_4)$ complexes were formed by the reactions between metal monoxides and CH_4 molecules, reactions 1 and 2, which were calculated to be exothermic:

$$MnO\ (^6\Sigma^+) + CH_4 \rightarrow OMn(CH_4)\ (^6A_1) \qquad \Delta E = -1.9\ \text{kcal/mol} \quad (1)$$

$$FeO\ (^5\Delta) + CH_4 \rightarrow OFe(CH_4)\ (^5A_1) \qquad \Delta E = -4.8\ \text{kcal/mol} \quad (2)$$

The $OMn(CH_4)$ and $OFe(CH_4)$ absorptions increased on annealing, suggesting that reactions 1 and 2 are barrier free.

The $OMn(CH_4)$ and $OFe(CH_4)$ complex absorptions decreased or disappeared upon broad-band irradiation, during which the CH_3MnOH and CH_3FeOH absorptions were produced. This suggests that the CH_3MnOH and CH_3FeOH molecules were generated from the $OMn(CH_4)$ and $OFe(CH_4)$ complexes via reactions 3 and 4.

$$OMn(CH_4)\ (^6A_1) \rightarrow CH_3MnOH\ (^6A') \quad (3)$$

$$OFe(CH_4)\ (^5A_1) \rightarrow CH_3FeOH\ (^5A') \quad (4)$$

According to our DFT/B3LYP calculations, the CH_3MnOH and CH_3FeOH molecules are 39.3 and 36.8 kcal/mol lower in energy than the $OMn(CH_4)$ and $OFe(CH_4)$ complexes, respectively.

The potential energy surfaces for the $MO^+ + CH_4 \rightarrow M^+ + CH_3OH$ reactions (M denotes first row transition metals) have been extensively studied.[6,7] The results showed that the reactions can occur by the following mechanism: $MO^+ + CH_4 \rightarrow OM^+(CH_4) \rightarrow TS1 \rightarrow CH_3M^+OH \rightarrow TS2 \rightarrow M^+(CH_3OH) \rightarrow M^+ + CH_3OH$. Crossings between the high-spin and low-spin potential energy surfaces were predicted to occur, and spin inversion can occur near a crossing region of potential energy surfaces. It can play a significant role in decreasing the barrier heights of the transition states. To get a better understanding of the reaction mechanism of the $MO + CH_4$ reactions, the potential energy surfaces along the $MO + CH_4 \rightarrow CH_3OH +$

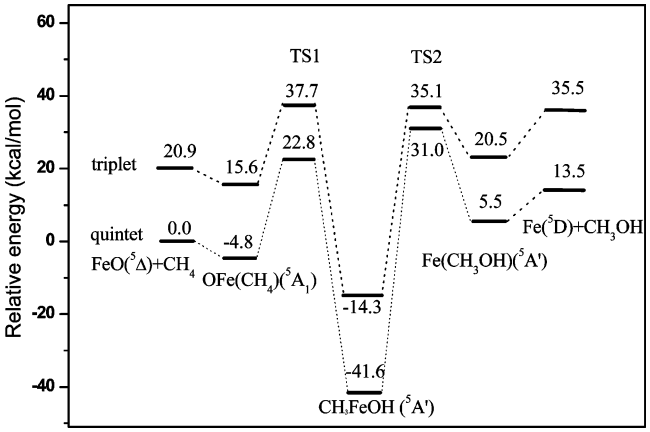

Figure 7. Profile of potential energy surface (in kcal/mol) of FeO + CH_4 reaction.

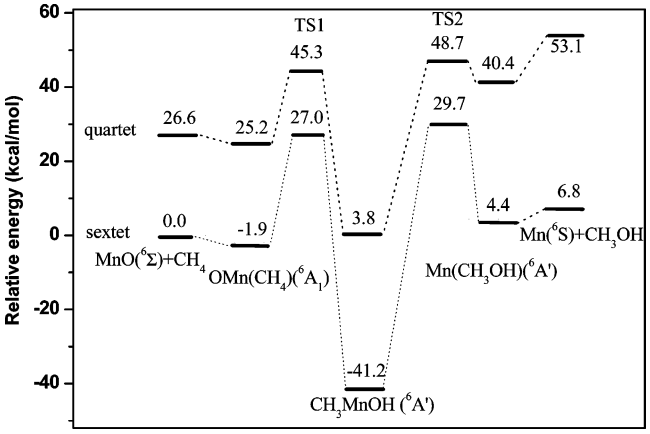

Figure 8. Profile of potential energy surface (in kcal/mol) of MnO + CH_4 reaction.

M reaction path have been computed at the B3LYP/6-311++G** level; the results are shown in Figures 7 and 8. We took quartet and sextet states for MnO, and triplet and quintet states for FeO, into account. All the reaction intermediates and transition states on the potential energy surfaces were fully optimized. As can be seen in Figures 7 and 8, the reactions follow mechanisms similar to those of the $MO^+ + CH_4$ reactions. The initial step of the reaction is the spontaneous formation of the $OM(CH_4)$ complex. The binding energies of 1.9 and 4.8 kcal/mol for MnO and FeO are significantly smaller than those for the corresponding monoxide cations (16.2 and 22.8 kcal/mol for MnO^+ and FeO^+)[6,7] and are even smaller than those of NiO and PdO (9−10 kcal/mol).[10,11]

From the complex, one hydrogen atom is passed from C to oxygen, leading to the CH_3MOH intermediate via a transition state (TS1). It is interesting to note that no spin crossing was observed for both the MnO and FeO reactions, which is quite different from the $MO^+ + CH_4$ reactions. The barrier heights at TS1 with respect to the $OM(CH_4)$ complex were predicted to be 28.9 and 27.6 kcal/mol for MnO and FeO, respectively. Yoshizawa et al. related the reaction efficiencies of transition metal oxide ions with methane to the barrier heights at TS1. The corresponding barrier heights for MnO^+ and FeO^+ were computed as 9.4 and 22.1 kcal/mol,[6,7] which indicates that the reaction efficiency for MnO and FeO should be lower than those for MnO^+ and FeO^+.

The potential energy surface for the FeO + $CH_4 \rightarrow CH_3$-FeOH reaction has previously been calculated by Yoshizawa et al. using the B3LYP functional as well.[7] They reported that the $OFe(CH_4)$ complex is 5.7 kcal/mol lower in energy than $FeO(^5\Sigma^+) + CH_4$. The ground state of FeO has been determined previously to be $^5\Delta$.[28,29] The $^5\Sigma^+$ state was calculated to lie 10.8 kcal/mol higher in energy above the $^5\Delta$ ground state. Moreover, Yoshizawa et al. predicted that the CH_3FeOH intermediate has a triplet ground state with a quintet state lying 28.5 kcal/mol higher in energy, and thus a spin crossing between the quintet and triplet potential energy surfaces occurred. Our calculations predicted that the CH_3FeOH intermediate has a quintet ground state with a triplet state lying 28.0 kcal/mol higher, and no spin crossing between the quintet and triplet potential energy surfaces was predicted.

The potential energy surfaces indicate that the formation of CH_3MOH from $OM(CH_4)$ requires activation energy, which is in accord with our experimental observations that the CH_3MOH molecules were only produced upon broad-band irradiation. In our experiments, the formation of CH_3MOH is a photochemical process, and most likely involves an electronically excited state of essentially MO, which is only weakly perturbed by the methane ligand. To define more closely the wavelengths of the light that promote rearrangement of $OM(CH_4)$ to CH_3MOH, experiments with selective irradiations were done. The results showed that only the UV light under the wavelength range of 250−300 nm could effectively initiate the rearrangement reactions. It is difficult to identify the most probable transitions because of the lack of UV absorption spectra in MnO and FeO: only some low-lying excited states have been reported.[30] Although the UV light could not initiate direct dissociation of CH_4 into CH_3 + H in the gas phase, the UV photon energy is sufficient for the dissociation. The electronic excitation energy of metal oxide may be redistributed to mobilize the hydrogen atom.

From the CH_3MOH intermediate, the reaction could further proceed by methyl group migration to form the $M(CH_3OH)$ complex via a transition state (TS2). This process was calculated to be endothermic. The barrier heights with respect to the CH_3-MOH intermediates were predicted to be 70.9 and 72.6 kcal/mol for MnO and FeO, respectively. These barrier heights are much higher than those at TS1. No $M(CH_3OH)$ or CH_3OH absorptions were observed in the experiments.

Conclusions

The reactions of transition metal monoxides (MnO and FeO) with methane molecules have been investigated using matrix isolation infrared absorption spectroscopy. The metal monoxide molecules were prepared by laser ablation of MnO_2 or Fe_2O_3 targets. The reaction intermediates and products were identified on the basis of isotopic substitution experiments with $^{13}CH_4$ and CD_4, as well as the density functional theoretical calculations. In solid argon, the manganese and iron monoxide molecules reacted with methane spontaneously on annealing to form the $OMn(CH_4)$ and $OFe(CH_4)$ complexes. Both complexes were predicted to have C_{2v} symmetry with the metal atom coordinated to two hydrogen atoms of the methane molecule. The binding energies with respect to the ground state reactants were predicted to be 1.9 and 4.8 kcal/mol, respectively, at the B3LYP/6-311++G** level. The $OMn(CH_4)$ and $OFe(CH_4)$ complexes underwent photochemical rearrangement to the CH_3-MnOH and CH_3FeOH molecules upon ultraviolet−visible irradiation. The calculation results also showed that no spin crossing occurred for both the MnO and FeO reactions, which is quite different from the $MO^+ + CH_4$ reactions. The barrier heights for conversion from the $OM(CH_4)$ complex to the CH_3-MOH intermediate were predicted to be 28.9 and 27.6 kcal/mol for MnO and FeO, respectively, higher than the corresponding barrier heights for MnO^+ and FeO^+.

Acknowledgment. We greatly acknowledge financial support from NSFC (20125311 and 20203005) and the NKBRSF of China.

Supporting Information Available: Fully optimized geometries of the stationary points and transition states in *xyz*-coordinates; calculated total energies, vibrational frequencies, and intensities. This material is available free of charge via the Internet at http://pubs.acs.org.

References and Notes

(1) Gesser, H. D.; Hunter, N. R.; Prakash, C. B. *Chem. Rev.* **1988**, *85*, 235.

(2) Schröder, D.; Fiedler, A.; Hrusak, J.; Schwarz, H. *J. Am. Chem. Soc.* **1992**, *114*, 1215. Ryan, M. F.; Fiedler, A.; Schröder, D.; Schwarz, H. *J. Am. Chem. Soc.* **1995**, *117*, 2033. Ryan, M. F.; Fiedler, A.; Schröder, D.; Schwarz, H. *Organometallics* **1994**, *13*, 4072. Schröder, D.; Schwarz, H. *Angew. Chem., Int. Ed.* **1995**, *34*, 1973.

(3) Schröder, D.; Schwarz, H. *Angew. Chem., Int. Ed. Engl.* **1990**, *29*, 1433.

(4) Clemmer, D. E.; Aristov, N.; Armentrout, P. B. *J. Phys. Chem.* **1993**, *97*, 544. Chen, Y. M.; Clemmer, D. E.; Armentrout, P. B. *J. Am. Chem. Soc.* **1994**, *116*, 7815.

(5) Aguirre, F.; Husband, J.; Thompson, C. J.; Stringer, K. L.; Metz, R. B. *J. Chem. Phys.* **2002**, *116*, 4071.

(6) Yoshizawa, K.; Shiota, Y.; Yamabe, T. *Chem. Eur. J.* **1997**, *3*, 1160. Yoshizawa, K.; Shiota, Y.; Yamabe, T. *J. Am. Chem. Soc.* **1998**, *120*, 564. Shiota, Y.; Yoshizawa, K. *J. Am. Chem. Soc.* **2000**, *122*, 12317.

(7) Yoshizawa, K.; Shiota, Y.; Yamabe, T. *Organometallics* **1998**, *17*, 2825.

(8) Broclawik, E.; Yamauchi, R.; Enduo, A.; Kubo, M.; Miyamoto, A. *J. Chem. Phys.* **1996**, *104*, 4098.

(9) Broclawik, E.; Yamauchi, R.; Enduo, A.; Kubo, M.; Miyamoto, A. *Int. J. Quantum Chem.* **1997**, *61*, 673.

(10) Hwang, D. Y.; Mebel, A. M. *Chem. Phys. Lett.* **2002**, *365*, 140.

(11) Hwang, D. Y.; Mebel, A. M. *J. Phys. Chem. A* **2002**, *106*, 12072.

(12) Xu, X.; Faglioni, F.; Goddard, W. A., III. *J. Phys. Chem. A* **2002**, *106*, 7171.

(13) Chen, M. H.; Wang, X. F.; Zhang, L. N.; Yu, M.; Qin, Q. Z. *Chem. Phys.* **1999**, *242*, 81. Zhou, M. F.; Zhang, L. N.; Shao, L. M.; Wang, W. N.; Fan, K. N.; Qin, Q. Z. *J. Phys. Chem. A* **2001**, *105*, 10747. Zhou, M. F.; Zhang, L. N.; Qin, Q. Z. *J. Phys. Chem. A* **2001**, *105*, 6407.

(14) Frisch, M. J.; Trucks, G. W.; Schlegel, H. B.; Scuseria, G. E.; Robb, M. A.; Cheeseman, J. R.; Zakrzewski, V. G.; Montgomery, J. A., Jr.; Stratmann, R. E.; Burant, J. C.; Dapprich, S.; Millam, J. M.; Daniels, A. D.; Kudin, K. N.; Strain, M. C.; Farkas, O.; Tomasi, J.; Barone, V.; Cossi, M.; Cammi, R.; Mennucci, B.; Pomelli, C.; Adamo, C.; Clifford, S.; Ochterski, J.; Petersson, G. A.; Ayala, P. Y.; Cui, Q.; Morokuma, K.; Malick, D. K.; Rabuck, A. D.; Raghavachari, K.; Foresman, J. B.; Cioslowski, J.; Ortiz, J. V.; Baboul, A. G.; Stefanov, B. B.; Liu, G.; Liashenko, A.; Piskorz, P.; Komaromi, I.; Gomperts, R.; Martin, R. L.; Fox, D. J.; Keith, T.; Al-Laham, M. A.; Peng, C. Y.; Nanayakkara, A.; Gonzalez, C.; Challacombe, M.; Gill, P. M. W.; Johnson, B.; Chen, W.; Wong, M. W.; Andres, J. L.; Gonzalez, C.; Head-Gordon, M.; Replogle, E. S.; Pople, J. A. *Gaussian 98*, revision A.7; Gaussian, Inc.: Pittsburgh, PA, 1998.

(15) Becke, A. D. *J. Chem. Phys.* **1993**, *98*, 5648.

(16) Lee, C.; Yang, E.; Parr, R. G. *Phys. Rev. B* **1988**, *37*, 785.

(17) McLean, A. D.; Chandler, G. S. *J. Chem. Phys.* **1980**, *72*, 5639.

(18) Krishnan, R.; Binkley, J. S.; Seeger, R.; Pople, J. A. *J. Chem. Phys.* **1980**, *72*, 650.

(19) Head-Gordon, M.; Pople, J. A.; Frisch, M. *Chem. Phys. Lett.* **1988**, *153*, 503.

(20) Chertihin, G. V.; Andrews, L. *J. Phys. Chem. A* **1997**, *101*, 8547.

(21) Hauge, R. H.; Margrave, J. L.; Kafafi, Z. H. In *Chemistry and Physcis of Matrix-Isolated Species*; Andrews, L., Moskovits, M., Eds.; North-Holland: Amsterdam, 1989; p 277.

(22) Kauffman, J. W.; Hauge, R. H.; Margrave, J. L. *J. Phys. Chem.* **1985**, *89*, 3541. Zhou, M. F.; Zhang, L. N.; Shao, L. M.; Wang, W. N.; Fan, K. N.; Qin, Q. Z. *J. Phys. Chem. A* **2001**, *105*, 5801.

(23) Chertihin, G. V.; Saffel, W.; Yustein, J. T.; Andrews, L. *J. Phys. Chem. A* **1996**, *100*, 5261.

(24) Billups, W. E.; Konarski, M. M.; Hauge, R. H.; Margrave, J. L. *J. Am. Chem. Soc.* **1980**, *102*, 7393.

(25) Zhang, L. N.; Zhou, M. F.; Shao, L. M.; Wang, W. N.; Fan, K. N.; Qin, Q. Z. *J. Phys. Chem. A* **2001**, *105*, 6998.

(26) Chen, M. H.; Huang, Z. G.; Zhou, M. F. *J. Phys. Chem. A* **2004**, *108*, 5950.

(27) Park, M.; Hauge, R. H.; Kafafi, Z. H.; Margrave, J. L. *J. Chem. Soc., Chem. Commun.* **1985**, 1570.

(28) Cheung, A. S. C.; Gordon, R. M.; Merer, A. J. *J. Mol. Spectrosc.* **1981**, *87*, 289. Cheung, A. S. C.; Lee, N.; Lyyra, A. M.; Merer, A. J. *J. Mol. Spectrosc.* **1982**, *95*, 213.

(29) Bauschlicher, C. W., Jr.; Langhoff, S. R.; Komornicki, A. *Theor. Chim. Acta* **1990**, *77*, 263. Gutsev, G. L.; Khanna, S. N.; Rao, B. K.; Jena, P. *J. Phys. Chem. A* **1999**, *103*, 5812.

(30) Wu, H. B.; Desai, S. R.; Wang, L. S. *J. Am. Chem. Soc.* **1996**, *118*, 5296. Gutsev, G. L.; Rao, B. K.; Jena, P.; Li, X.; Wang, L. S. *J. Chem. Phys.* **2000**, *113*, 1473.